Subtype selectivity and flexibility of ionotropic glutamate receptors upon antagonist ligand binding

Ulla Pentikäinen,†[a,b] Luca Settimo,†[a] Mark S. Johnson[a] and Olli T. Pentikäinen*[a]

Received 25th October 2005, Accepted 10th January 2006
First published as an Advance Article on the web 26th January 2006
DOI: 10.1039/b515111b

The binding modes of a set of known *ionotropic* glutamate receptor antagonist-ligands have been studied using homology modeling, molecular docking, molecular dynamics (MD) simulations and *ab initio* quantum mechanical calculations. The core structure of the studied ligands is the decahydroisoquinoline ring, which has a carboxylic acid group at position three and different negatively-charged substituents (R) at position six. The binding affinities of these molecules have been reported earlier. From the current study, the carboxylate group of the decahydroisoquinoline ring hydrogen bonds with Arg485, the amino group with Pro478 and Thr480, and the negatively charged substituent R interacts with the positively charged N-terminus of helix-F. The subtype selectivity of these ligands seems to be strongly dependent on the amino acid at position 650 (GluR2: leucine, GluR5: valine), which affects the conformation of the ligand and ligand–receptor interactions, but depends considerably on the size of the R-group of the ligand. In addition, the MD simulations also revealed that the relative positions of the S1 and S2 domains can alter significantly showing different "closure" and "rotational movements" depending on the antagonist-ligand that is bound. Accordingly, molecular docking of antagonist ligands into static crystal structures cannot sufficiently explain ligand binding and subtype selectivity.

Introduction

The *ionotropic* glutamate receptors (iGluRs) can be divided, based on agonist binding affinities, into three subclasses: *N*-methyl-D-aspartic acid (NMDA; NR1–3 subunits), (*S*)-2-amino-3-(3-hydroxy-5-methyl-4-isoxazolyl)propionic acid (AMPA; GluR1–4) and kainic acid (KA; GluR5–7 and KA1–2) receptors. These receptors play an important pharmacological role in many processes and when over-activated they cause neuronal degeneration.[1,2] As different glutamate receptors have different functions and roles in disease processes,[3–6] the development of effective antagonist-ligands, which can discriminate between different glutamate receptors, has been the focus of extensive research. Derivatives of decahydroisoquinoline comprise one set of antagonist-ligands that are subtype-selective for different iGluRs.[7–10] Compounds from the decahydroisoquinoline series have also been reported to have potential in the treatment of several diseases; for example, some GluR2-selective decahydroisoquinoline derivates are neuroprotective and, therefore, may have use in the treatment of ischemic conditions,[7,8] and GluR5-selective molecules have, in turn, demonstrated efficacy towards epilepsy[9] and migraine.[10] In contrast to several other antagonists, decahydroisoquinoline derivatives have good water solubility, which would help in their clinical use.[7] However, the binding mode of these ligands into iGluRs is not known.

Three-dimensional structures of an iGluR with a bound antagonist ligand have been published only for the ligand binding domain (LBD) of GluR2 with bound 6,7-dinitro-2,3-dihydroxyquinoxaline (DNQX)[11] and 2-amino-3-[5-*tert*-butyl-3-(phosphonomethoxy)-4-isoxazolyl]propionic acid (ATPO)[12] and for the LBD of NR1 with bound 5,7-dichlorokynurenic acid (DCKA).[13] Each of these structures shows a high degree of opening of domain S1 *versus* S2 in comparison to agonist-bound structures.[11–15] In addition, based on various experimental studies [X-ray crystallography,[11–13,15] solution X-ray scattering,[16,17] nuclear magnetic resonance (NMR)[14,18–22] and using other spectroscopic methods[23–25]] and on modeling studies [molecular dynamics (MD)][26–29] and structural comparison,[30] antagonist-bound structures have displayed different degrees of S1–S2 domain opening.

The interactions between an antagonist ligand and receptor are strongly dependent on the three dimensional shape of the ligand: ATPO forms strong electrostatic interactions with the N-terminus of helix-F (helix-F: Gly653–Ser662), Arg485 and Glu705 (Fig. 1), whereas DNQX and DCKA, which are both fairly planar ligands,

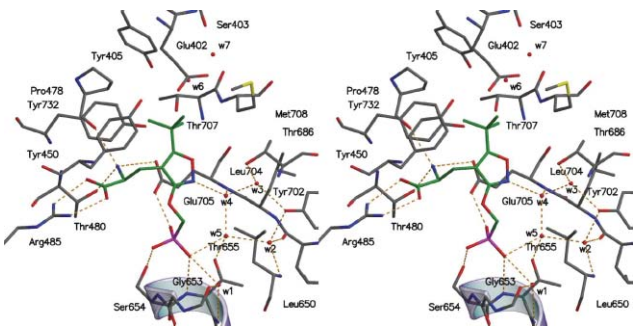

Fig. 1 Key interactions (hydrogen bonds, orange dotted lines) at the binding site of the GluR2–ATPO crystal structure (in stereo). The silver spiral highlights the N-terminus of helix-F. In addition, the important water molecules (w1–w5) are shown.

[a]*Department of Biochemistry and Pharmacy, Åbo Akademi University, Tykistökatu 6A, FIN-20520, Turku, Finland. E-mail: olli.pentikainen@csc.fi; Fax: +358-2-215-3280; Tel: +358-40-521-6913*
[b]*Department of Chemistry, University of Turku, Vatselankatu 2, FIN-20014, University of Turku*
† These authors made an equal contribution to this work.

Table 1 The ligand binding affinities (K_i/nM) for GluR2 and GluR5 for the studied ligands

Ligand	GluR2	GluR5
I	3200[a]	4200[a]
	3250[b]	4880[b]
II	820[b]	3410[b]
III	6250[b]	370[b]
IV	117000[a]	156[a]
V	37120[b]	1010[b]
VI	36400[b]	2620[b]

[a] Data taken from ref. 10 [b] Data taken from ref. 7

lack the interaction with the N-terminus of helix-F and, thus, interactions with the receptors are quite different from those of ATPO. Water molecules also have critical roles in ligand binding (Fig. 1). Notably, water molecules w1 and w2 (Fig. 1) are seen in all published crystal structures (see *e.g.* ref. 11). Water molecule w4 interacts with the main-chain amino group of Glu705 and the bound ligand (*e.g.*, ATPO), and can be replaced by the ligand when a ligand can directly accept a hydrogen bond from the main-chain amino group of Glu705 (*e.g.*, AMPA). Water w5, accepting a hydrogen bond from the hydroxyl group of Thr655, is observed less often since ligands usually occupy that space.

In the present work, the binding of a set of decahydroisoquinoline molecules (Fig. 2), which are known to be selective antagonists for GluR2 or GluR5[7,10] (Table 1) and potential antagonist molecules for the treatment of several diseases, has been studied by the means of homology modeling, molecular docking, MD simulations and quantum mechanical calculations. The experimental binding affinities for these molecules on *homomeric* iGluRs (Table 1) have been reported earlier.[7,10] We have constructed binding motifs (relative positioning of a ligand in the ligand-binding site and the physicochemical interactions that take place) for these antagonist-ligands and found plausible explanations for ligand-binding selectivity among the different iGluRs. An analysis of this kind should yield information that would facilitate the design of new, more effective subclass- and subunit-selective antagonist-ligands for iGluRs.

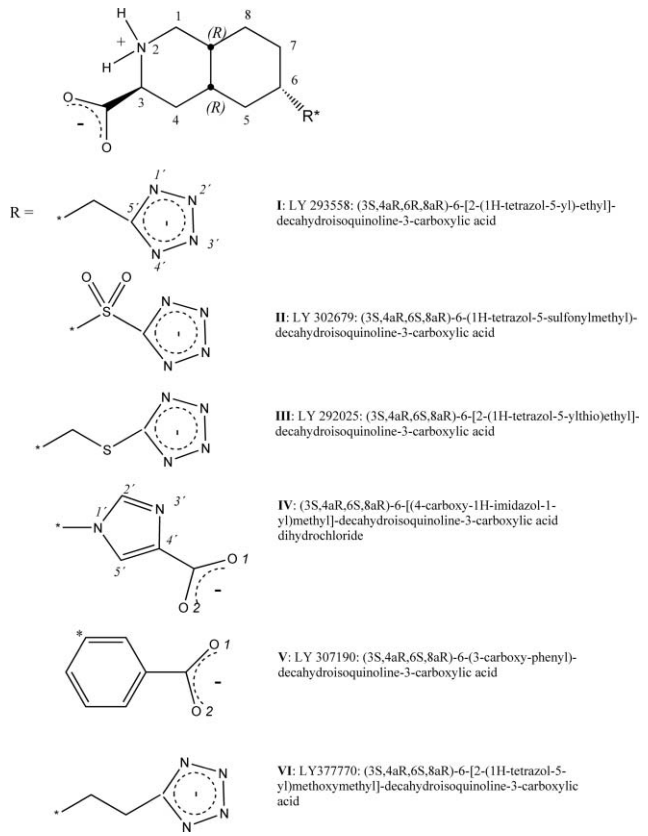

Fig. 2 The structures, IUPAC names and LY-numbers of the decahydroisoquinoline molecules (**I–V**) studied. Compound **VI** is shown for reference.

Results and discussion

Ligands studied

The antagonist ligands **I–V**, whose modes of binding to the GluR2 and GluR5 receptors were studied, are shown in Fig. 2, and their experimentally determined binding affinities obtained from the literature are listed in Table 1. All ligands consist of a decahydroisoquinoline bicyclical ring having a carboxylic acid group at position three and a substituent *R* at the position six (Fig. 2). The substituent *R* at position six of the decahydroisoquinoline ring differs for all of the ligands. Ligands **I–III** have a tetrazole group attached *via* a linker to the decahydroisoquinoline ring. **I** has a CH_2–CH_2-linker, whereas in **II** the CH_2-group next to the decahydroisoquinoline ring has been replaced with a sulfonyl group. The linker of **III** is longer than those in **I** and **II**, having two CH_2-groups and a sulfur atom next to the decahydroisoquinoline ring. Ligand **IV** has 4-carboxy-1H-imidazole attached *via* one CH_2-group to the decahydroisoquinoline ring, and **V** has a 3-carboxy-phenyl group directly attached to the decahydroisoquinoline core ring.

The binding affinities of ligands **I–V** to GluR2 and GluR5 (Table 1) have been determined at pH 7.5. Therefore, all carboxyl-groups and amino groups were modeled in the ionic forms. All tetrazole groups were assumed to be negatively charged under experimental conditions, since the pK_a value for tetrazole is 4.9.[31] Similarly, the 3′ nitrogen in the imidazole ring of **IV** (Fig. 2) was assumed to be unprotonated at pH 7.5, since the pK_a value of the nitrogen atom of a similar structure (1-methylimidazole-4-carboxylic acid) is 5.7.[32]

Protein models

The crystal structure of the ligand binding domain of GluR2 in complex with the antagonist ligand ATPO (PDB code: 1n0t[12]) was used as a starting structure for GluR2–ligand complexes and as a template structure to build protein models of different extracellular domains of the AMPA/KA receptors. This X-ray structure was chosen since the binding characteristics of the decahydroisoquinolines were expected to be more similar to those of ATPO than those of DNQX. Model structures for all of the other AMPA/KA receptors were built with Homodge in the Bodil Modeling Environment[33] using the multiple sequence alignment of the AMPA/KA receptors made with Malign in Bodil (Fig. 3). The sequence identity varies from approximately 90% (among the AMPA receptors: GluR1–4) to about 50% (between GluR2 and the KA receptors: GluR5–7 and KA1–2), thus, the quality of the sequence alignment is high enough to produce reliable homology models. The recently published crystal structures of GluR5 with

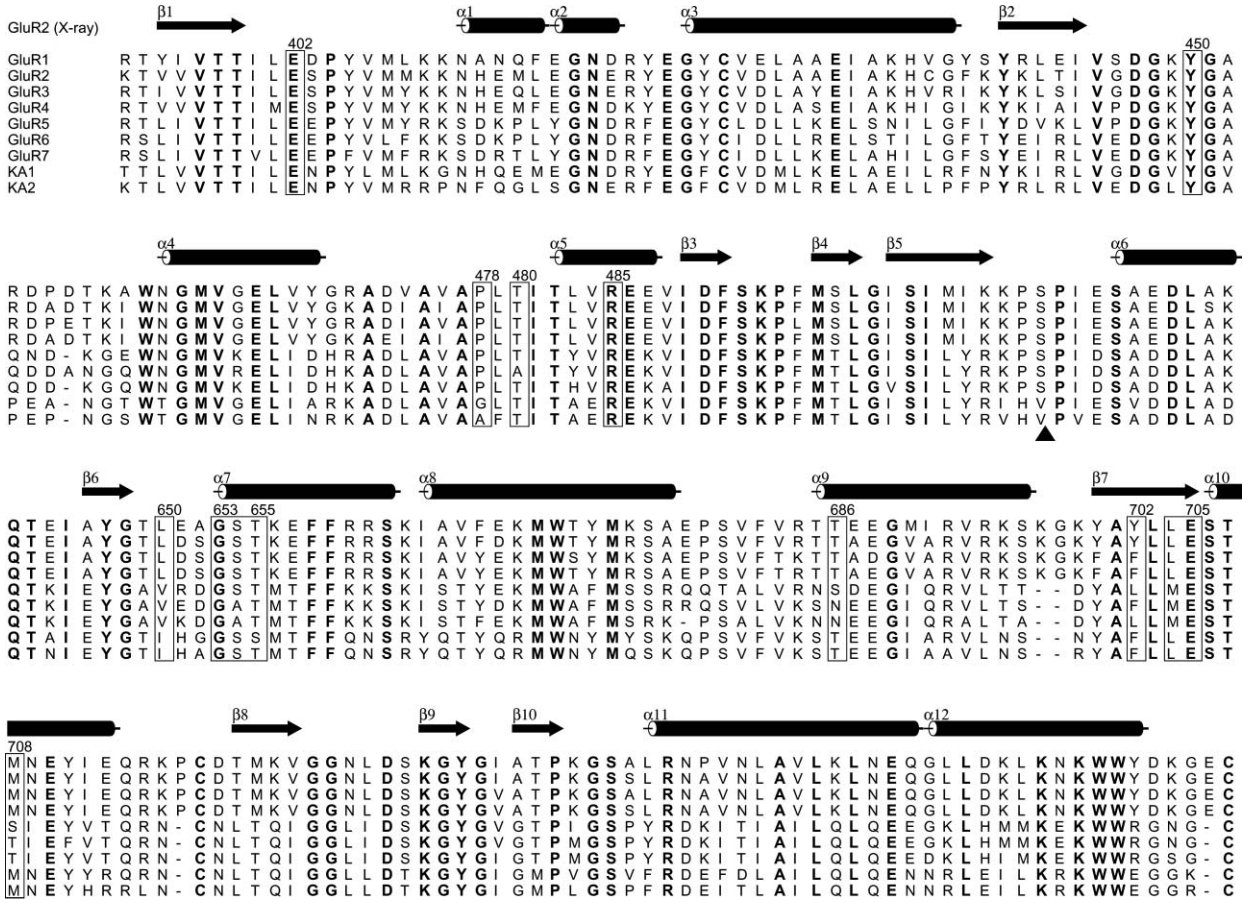

Fig. 3 Sequence alignment of the LBDs of rat AMPA (GluR1–4) and KA receptors (GluR5–7 and KA1–2) (triangle indicates the S1–S2 junction). Residues within the ligand-binding pocket are boxed; conserved residues are shown in bold type; the secondary structure and residue numbering are from the GluR2 crystal structure (PDB code: 1n0t[12]).

bound agonist ligands[34,35] cannot be used in studies of antagonist ligands **I–V**, because of different closure state of S1–S2 domains. However, as the amino acid side chain conformations are highly similar for GluR2 with bound agonist and antagonist ligands, it can be assumed that also the amino acid conformations of GluR5 would be highly similar in both agonist and antagonist ligand bound conformations. Because our GluR5 model structure has similar side chain conformations as seen in the published crystal structures of GluR5 with bound agonist ligands,[34,35] it can be assumed that the quality of the model structure is high enough to be used in the antagonist ligand binding studies. For clarity, we have used GluR2 numbering throughout the text.

Binding mode of the decahydroisoquinoline-3-carboxylic acid core structure in GluR2 and GluR5

The conformations of ligands **I–V** were optimized quantum mechanically, first *in vacuo* and then using a continuum solvent model ($\varepsilon = 80$, water). The bicyclical ring in all compounds was observed to adopt a chair–chair conformation. In order to compare the theoretically calculated conformation of the decahydroisoquinoline structure to those determined experimentally, similar (sub)structures to decahydroisoquinoline-3-carboxylic acid having a substituent at position six were identified within the Cambridge Structural Database (CSD).[36] The majority of such structures display a similar chair–chair conformation as obtained from quantum mechanical calculations. The same chair–chair conformation was also seen in the structure of decahydroisoquinoline-3(*S*)-carboxylic acid determined using nuclear magnetic resonance.[37] Accordingly, the chair–chair conformation seems to be the lowest energy conformation of the decahydroisoquinoline ring. However, the bioactive conformation is not necessarily at the global energy minimum, and therefore several bicyclical ring conformations were built with Corina,[38,39] and they were docked into GluR2.

The docking of decahydroisoquinoline structures with different ring conformations revealed that in the chair–chair conformation the decahydroisoquinoline can form more strong interactions than with other ring–ring conformations. The interactions that are seen for docked decahydroisoquinoline chair–chair conformation are (i) the carboxylate group at position three interacts with the guanidinium group of Arg485, and (ii) the amino group at position two interacts with both the main-chain carbonyl oxygen atom of Pro478 and the side-chain hydroxyl-group of Thr480 (Fig. 4). The interaction of the ligand carboxylate with Arg485 is seen in all crystal structures of GluR2 with bound ligand.[11] The amino group interactions with the modeled structures are also found in the crystal structures of iGluRs with bound ligands: the secondary amine found in KA (bound into GluR2)[11,40] and in domoic acid (bound into GluR6)[41] interacts with the carbonyl oxygen atom of Pro478 and the carboxyl-group of Glu705, whereas the primary

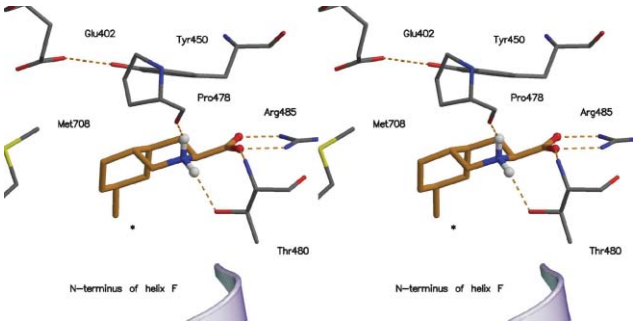

Fig. 4 Essential interactions of the core structure of decahydroisoquinoline in the binding pocket of GluR2 (in stereo). The hydrogen bonds established by the carboxylate and amino groups are shown with orange dotted lines. The star indicates the position where substituents of the studied ligands are attached (see Fig. 2).

amine (*e.g.*, GluR2–GLU,[11] GluR2–ATPO[12]) forms an additional interaction with the hydroxyl-group of Thr480. Accordingly, based on the experimentally observed interactions seen in the X-ray structures and conformations of similar structures in the literature,[36,37] it can be assumed that the decahydroisoquinoline-3-carboxylate binds to iGluRs in a chair–chair conformation forming polar interactions with Arg485, Pro478 and Thr480.

Binding mode of ligands I–V in GluR2 and GluR5

Quantum mechanically optimized structures of ligands **I–V** were docked into the crystal structure of GluR2 and into the model structure of GluR5. Several side chain conformations for various amino acids at the ligand binding site were tested, especially for those amino acids that differ between GluR2 and GluR5. In all cases, the decahydroisoquinoline ring adopted the chair–chair conformation and the 3-carboxylate and 2-amino groups form similar interactions as observed in the docking of 3-carboxy-decahydroisoquinoline. In contrast to our previous study of agonist ligand binding and subtype selectivity,[43] where homology modeling and docking were able to produce receptor–ligand complexes that explain the subtype selectivity, in this study the antagonist ligand conformations achieved from docking were not able to explain the experimentally observed differences in the binding affinities. Therefore, MD simulations were performed on all of the modeled complexes. The best ligand conformation from docking simulations was selected as a starting structure for MD simulation. This selection was based on the following criteria: (a) 3-carboxylate group of ligands has to be in close proximity to Arg485, (b) 2-amino group of ligands has to be in close proximity to main chain carbonyl oxygen atom of Pro478 and hydroxyl group of Thr480, (c) the R-group of ligands has to be positioned in such way that it has at least some favorable polar interactions with the receptor, in practice either with main chain amino group of Glu705 or with main chain amino group and side chain hydroxyl group of Thr655, and (iv) the fitness values given by Gold. However, with ligand **II** in complex with GluR5, a different starting conformation was selected (see below), in order to investigate the effect of the starting structure on the result of MD simulation. The stability of protein structures during the MD simulations was examined by measuring the time evolution of the root mean square deviation (RMSD) of the C^{α} atoms. According to RMSD curves, stable trajectories are obtained, where the RMSD varies between 1.5–2.5 Å (data not shown). Since water molecules play an important role in ligand binding, methods such as MM-PBSA,[42] which uses a continuum solvent model, cannot be applied for binding energy estimations. Similarly, the empirical scoring functions cannot be used because they do not take into account the solvent molecules and they cannot reliably evaluate the internal energy of ligand and receptor. Therefore, the binding mode of each ligand was analyzed by comparing experimentally determined K_i-values to observed interactions in the modeled complexes (Figs. 5–9; Table 1) and internal energies of ligands calculated with density functional theory (Table 2).

Table 2 Differences in the internal energies (kcal mol^{-1}) for ligand conformations obtained from the MD simulations

Ligand	I	II	III	IV	V
$\Delta E_{internal}$(GluR2–GluR5)	−3.0	−3.8	9.0	−1.0	4.2

The internal energies for each ligand are calculated as average energies for 27 structures with 15 ps time intervals during the last 450 ps of total simulation time. Internal energies are calculated with B3LYP/6-31 + G*. $\Delta E_{internal}$(GluR2–GluR5) = $E_{internal}$(GluR2)–$E_{internal}$(GluR5). Standard deviation for internal energies for each ligand was less than 1%.

Ligand I

The binding mode obtained from docking of **I** into GluR2 is shown in Fig. 5a. A very similar conformation for **I** was also obtained in the GluR5–**I** complex (not shown). In both cases, the 1′ nitrogen atom forms a hydrogen bond with the hydroxyl group of Thr655 and the 2′ nitrogen atom with the main-chain amino group of the same residue (Fig. 5a).

During the MD simulation, **I** as a complex with GluR2 adopts a more extended conformation when compared to the starting structure of the complex (Fig. 5b). This extended conformation becomes possible due to rotation of the S2 domain such that helix-F and helix-H (helix-H:Thr685–Ser696) move with respect to the S1 domain (see Fig. 5c). Consequently, the distance between the domains increases from 9 Å to 10 Å (measured as the distance between the C^{α}-atom of Ser654 and the C^{ζ}-atom of Arg485). The resulting conformation of the receptor closely resembles that of the NR1 receptor with bound DCKA (PDB access code: 1pbq[13]), instead of GluR2 receptor with ATPO that was used as a starting structure (Fig. 5d).

In the extended conformation obtained from the MD simulation (Fig. 5b), the tetrazole ring is stabilized from one side by electrostatic interactions with the hydroxyl and main-chain amino group of Thr655 and from the other side by the main-chain amino group of Glu705 (Table 3). None of these interactions can be considered as strong hydrogen bonds since the angles between the acceptors and donors are not optimal for hydrogen bonding (Table 3). However, the alkyl linker is very flexible, allowing for alternative orientations of the tetrazole ring, which, in turn, can enforce strong interactions to either Thr655 or Glu705, but not both of them at the same time. In Fig. 5b is shown the average structure (over the last 450 ps of the total simulation time), which is, in addition to hydrogen bonds, stabilized by the packing of Leu650 against the planar face of the tetrazole ring. This hydrophobic packing is also seen in those ligand conformations where tetrazole ring position is stabilized by the main chain amino

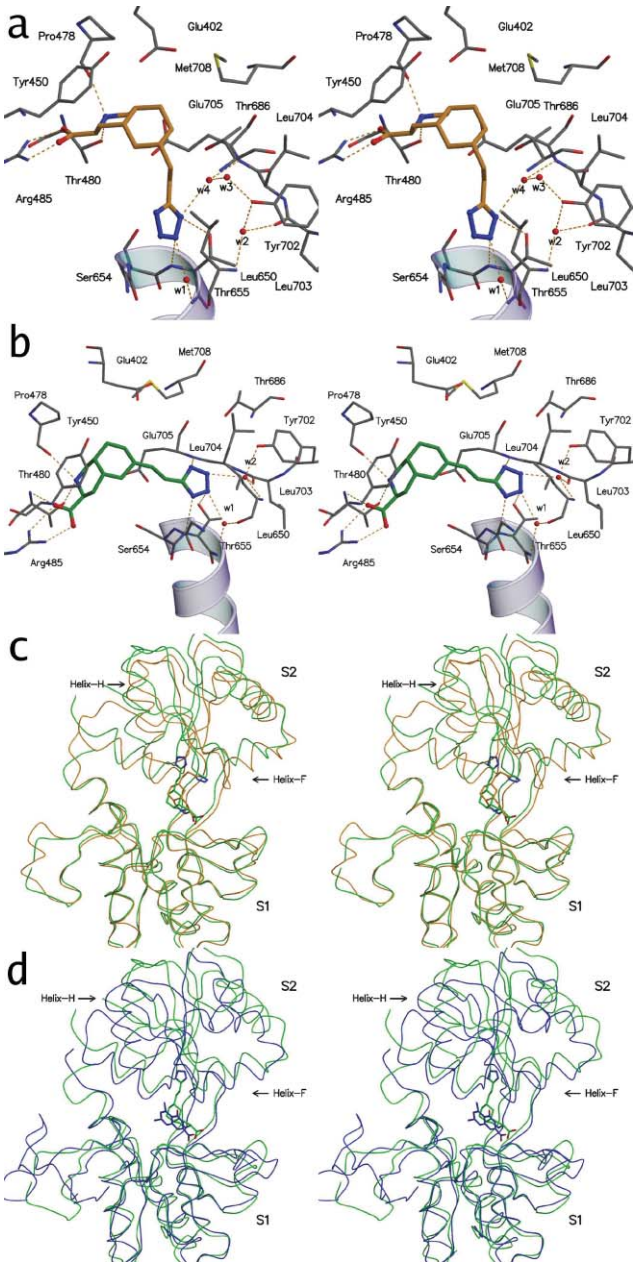

Fig. 5 The binding conformation of **I** as well as the changes in receptor conformation during the MD simulation. While (a) the docked conformation of **I** (orange carbon atoms) into GluR2 is bent, the (b) conformation of **I** after MD simulation (green carbon atoms) is in a more relaxed form. The essential hydrogen bonds are shown with orange dotted lines. In (c) the relative movement of domain S2 and the change in the ligand conformation are shown (starting structure: orange trace and orange carbon atoms; simulated structure: green trace and green carbon atoms). (d) The receptor conformation after MD simulation (green trace and green atoms) is highly similar to that of the crystal structure of NR1 in complex with DCKA (blue trace and blue carbon atoms). The protein structures in (c) and (d) are superimposed over C^{α} atoms of the S1 domain and helices F and H are indicated with arrows.

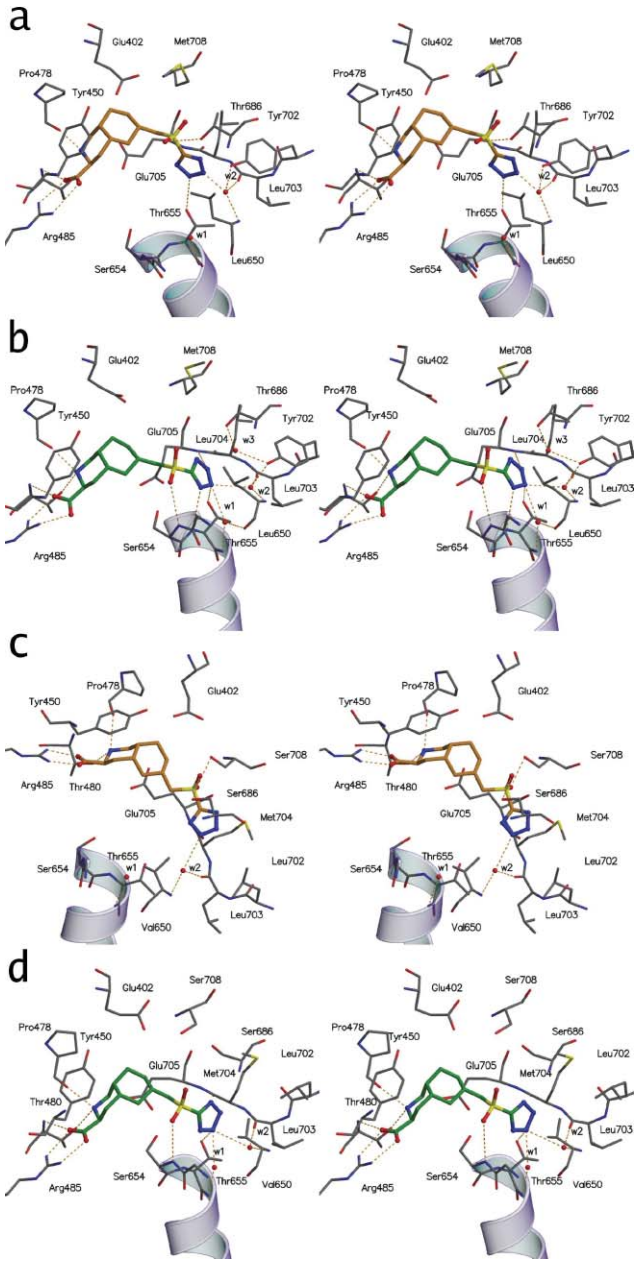

Fig. 6 Docking of **II** (orange carbon atoms) into (a) GluR2 and (c) GluR5 resulted in conformations where the interaction with helix-F was absent. However, during the MD simulation the ligand takes on a conformation highly similar to that seen with **I** (see Fig. 5). Even though the interactions of **II** (green carbons) are highly similar with (b) GluR2 and (d) GluR5, the packing with the receptor is different. The essential hydrogen bonds are shown with orange dotted lines.

group of Glu705 or the side-chain hydroxyl and main-chain amino group of Thr655 (data not shown). In addition, water molecules w1 and w2 hydrogen bond with the tetrazole ring regardless of the changes in the conformation of the ligand (Table 3; Fig. 5b).

The starting structure of **I** in complex with GluR5 is similar to that in the complex with GluR2. When compared to the starting structure, during the MD simulation the receptor–ligand complex undergoes a smaller conformational change than was seen for the GluR2–**I** complex. Both the degree of rotation and the distance between the S1 and S2 domains are smaller than with GluR2. Therefore, the shape of the ligand binding pocket is different and the ligand consequently must adopt a less extended conformation than with GluR2. In addition, the tetrazole ring is in different orientations in GluR2 and GluR5; in GluR2 the plane of the

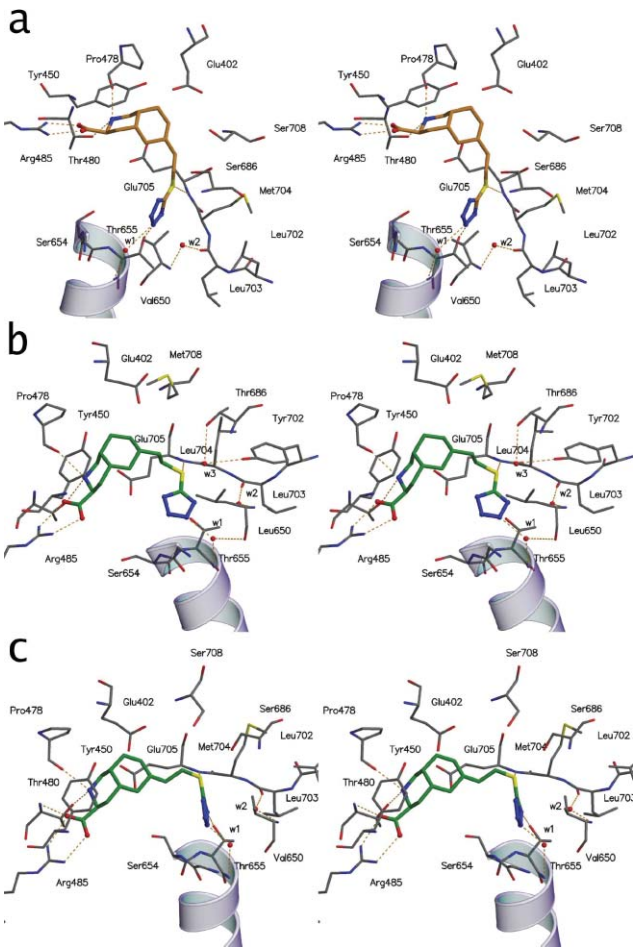

Fig. 7 Docking of **III** into both GluR2 (not shown) and (a) GluR5 results in highly similar conformations. During the MD simulation both the receptor and ligand conformations remained quite similar as in the starting structure, however, (b) Leu650 of GluR2 forces the ligand to have an unfavorable intramolecular conformation in contrast to (c) GluR5 where valine is seen at position 650. The essential hydrogen bonds are shown with orange dotted lines.

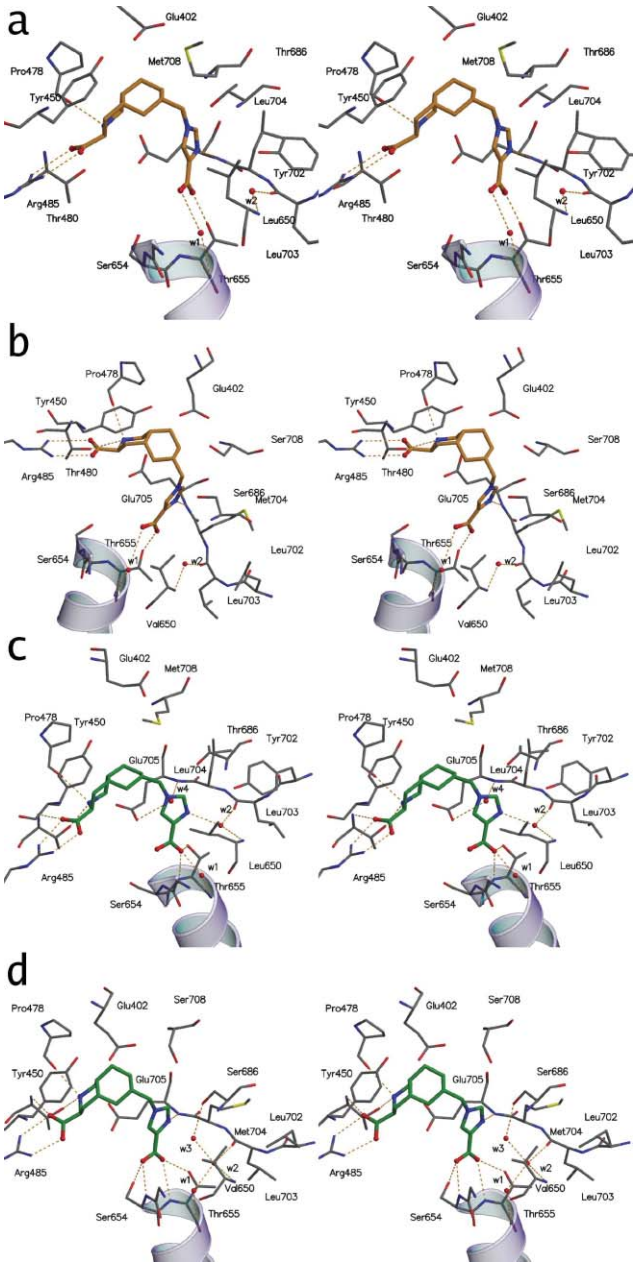

Fig. 8 Docking of **IV** to GluR2 (a) and GluR5 (b) results in highly similar conformations. However, in GluR2 (a) Leu650 forms unfavorable interactions with both Tyr702 and the bound ligand; thus, (c) during the MD simulation both the ligand and the receptor alter their conformation but cannot form good mutual interactions. (d) In contrast, all possible interactions of **IV** with GluR5 are optimized. The essential hydrogen bonds are shown with orange dotted lines.

tetrazole ring is parallel with the plane of decahydroisoquinoline, whereas in GluR5 the tetrazole ring is oriented perpendicular to the decahydroisoquinoline ring. These differences are also reflected in the internal energy of the ligand, which is 3.0 kcal mol^{-1} (Table 2) more unfavorable with GluR5 than with GluR2. The interactions between the ligand and GluR5 also differ from those seen with GluR2. With GluR5 the tetrazole ring forms only one, but strong, hydrogen bond with the receptor (from N2′ to the OH of Thr655; Table 3), while the other interactions seen with GluR2 are not present. In addition, the favorable packing of Leu650 is not seen with GluR5 since leucine is replaced by smaller valine.

In summary, the conformation of **I** differs for GluR2 and GluR5 and **I** does not seem to form very strong interactions with either of the receptors: with GluR2 there are several weak interactions, whereas with GluR5 one strong hydrogen bond is formed. In addition to the explained effect of Leu → Val at position 650 (GluR2 → GluR5) difference at the binding site, the other sequence differences between the receptors can explain partially the observed differences in experimental ligand binding affinities. The methionine side chain at position 708 at GluR2 can pack against the core of the ligand (Fig. 5b), while serine that is seen in the equivalent position in GluR5 could not do this. The other differences, Thr686Ser, Tyr702Leu and Leu704Met (GluR2 → GluR5), do not clearly affect the ligand binding, even though that the Tyr702 in GluR2 might help on stabilization of water w2 position (Fig. 5b). These observations are consistent with the experimental binding affinities (Table 1), which show that binding of **I** is weak into both receptors, but slightly favors GluR2.

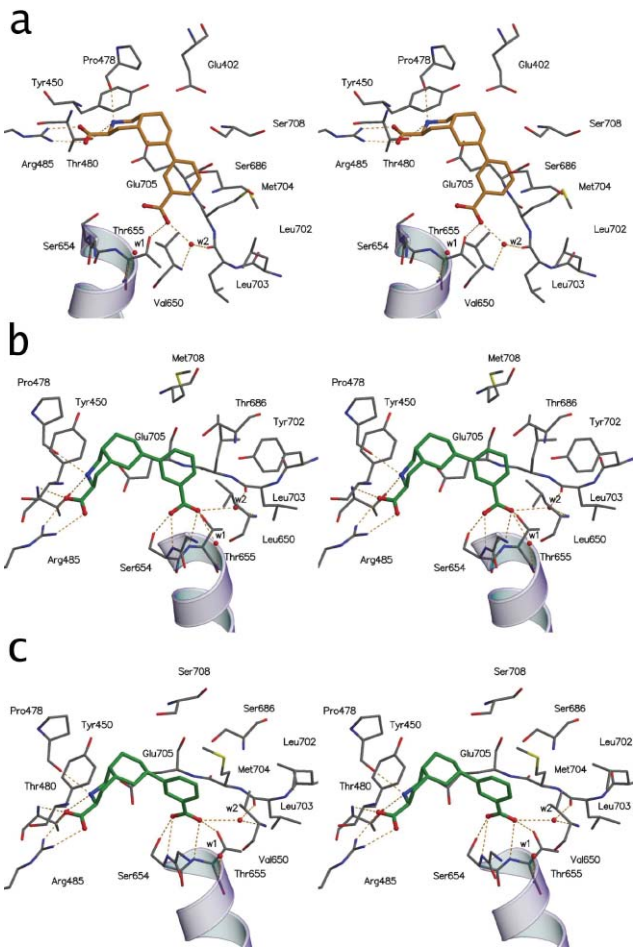

Fig. 9 Docking of **V** to GluR2 (not shown) and GluR5 (a) results in highly similar binding conformations. The conformation are not favorable, and thus, during the MD simulation the phenyl ring tries to change its conformation from the perpendicular to the diagonal orientation with respect to the bicyclic ring. In (b) GluR2 this rotation cannot take place due to the presence of Leu650, while in GluR5 (c) it can because position 650 is occupied by smaller valine. The essential hydrogen bonds are shown with orange dotted lines.

Ligand II

Molecule **II** is the most GluR2-selective ligand among the compounds studied, although the selectivity is rather modest, GluR2 binding is only approximately 4-fold better than to GluR5 (Table 1). **II** also has the highest affinity for GluR2 among the compounds studied; **II** binds *e.g.* four times stronger to GluR2 than **I** does. Docking of **II** into GluR2 resulted in the conformation shown in Fig. 6a. In this conformation, two hydrogen bonds between **II** and GluR2 are observed: from the 2′ nitrogen atom of the tetrazole ring to the hydroxyl group of Thr655 and from the sulfonyl group and the hydroxyl group of Thr686. The water molecule, w2, stabilizes the docked conformation. Leu650 also packs favorably with the planar, hydrophobic face of the tetrazole group. However, the conformation is not optimal, because the negatively charged tetrazole ring is positioned very close to the oxygen atom of the hydroxyl group of Tyr702. In addition, the polar sulfonyl group is only partially solvated, where only one of two oxygen atoms is oriented towards the solvent and the other is buried by the surrounding amino acid residues (Thr686 and Met708).

During the MD simulation of the GluR2–**II** complex, similar conformational changes were seen for both the receptor and the ligand (Fig. 6b) as for the GluR2–**I** complex (Fig. 5b). This is expected since both of these ligands have an equal length linker. The conformation of GluR2–**II** complex obtained from the MD simulation (Fig. 6b) allows the formation of more favorable interactions than are seen in the starting structure (Fig. 6a), bringing the negatively charged tetrazole ring into close proximity of the positively charged end of helix-F. In addition to the hydrogen bond between atom N3′ of the tetrazole ring and the hydroxyl group of Thr655 seen in the starting structure, atom N4′ hydrogen bonds with the main-chain amino group of the same residue, and a weak hydrogen bond forms between atom N2′ and the main-chain NH group of Glu705 (Table 3). The water molecules w1 and w2 stabilize the ligand conformation. The orientation of the linker also changes, such that the sulfonyl group turns towards helix-F forming a hydrogen bond with the main-chain amino group of Ser654 as opposed to the hydroxyl group of Thr686 in the starting structure. As a consequence of the linker orientation, both oxygen atoms of the sulfonyl group are exposed to solvent, which has a favorable contribution to the ligand binding energy. In addition, in the structure obtained from the MD simulation, hydrophobic interactions between the side chain of Leu650 and the hydrophobic planar face of the tetrazole-ring, contributes favorably towards the binding energy.

The conformations obtained from the MD simulation of GluR2–**I** and GluR2–**II** are consistent with the observed K_i-values, which show that **II** binds four times stronger to GluR2 than **I** does (Table 1). The tetrazole ring of **II** forms two hydrogen bonds and electrostatic interaction with the receptor and also the sulfonyl group hydrogen bonds with the receptor, whereas with **I** the tetrazole ring is only stabilized by electrostatic interactions, not optimal hydrogen bonds (Table 3). The interactions with water molecules are highly similar with both **I** and **II**. For **II** the solvation of the sulfonyl group adds an additional favorable impact for the ligand binding.

With GluR5, the starting conformation of **II** was selected in a way that the sulfonyl group interacts with Ser686 and Ser708 (Fig. 6c). This was done in order to study whether these residues could stabilize a ligand conformation in a different way from that seen with GluR2. However, during the MD simulation the conformation of **II** in complex with GluR5 changes (Fig. 6d) and closely resembles the conformation seen with GluR2 (Fig. 6b). Like for GluR2, the sulfonyl group forms a hydrogen bond with the main-chain amino group of Ser654 of helix-F, and also the tetrazole ring interacts with helix-F. However, the interactions between receptor and the tetrazole ring are different with GluR2 and GluR5 (Table 3). With GluR2, the tetrazole ring forms two hydrogen bonds with helix-F, whereas with GluR5 only one hydrogen bond is formed between atom N3′ and the hydroxyl group of Thr655 (Table 3). In addition, with GluR2, the tetrazole ring also interacts with the main-chain amino group of Glu705, which is not present with GluR5. The absence of these interactions with GluR5 can be explained by the presence of the smaller valine side chain (residue 650) as opposed to leucine in GluR2. Accordingly, in GluR5 there is more space in the cavity between helix-F and helix-H, and the tetrazole group of **II** can extend deeper into the cavity, and interactions similar to those seen with

GluR2 are not possible. Furthermore, in GluR2, bulkier leucine at position 650 packs better with the hydrophobic face of tetrazole than smaller valine in GluR5, the former giving a favorable contribution to the total binding energy. The internal energy of conformation of **II** in GluR2 is 3.8 kcal mol^{-1} more favorable than in GluR5 (Table 2). The experimentally observed difference in the binding affinity between GluR2 and GluR5, approximately 4-fold, seems to be due to the sequence difference at position 650, which leads to different interactions and conformations of the ligand. In addition, Tyr 702 in GluR2 can stabilize the water molecule w3 together with the side chain hydroxyl-group of Thr686 (serine in GluR5) and might thus, affect favorably the enthropy contribution of ligand binding, while leucine in equivalent position in GluR5 cannot do this. The structures obtained from MD simulation are consistent with the experimental observation that **I** and **II** bind equally well to GluR5, since the R-groups of both ligands form two hydrogen bonds with receptor.

Ligand III

III binds selectively to GluR5, binding being 17-fold better than for GluR2 (Table 1). Structurally, **III** differs from the other decahydroisoquinoline compounds by having the longest linker, $–CH_2–CH_2–S-$, among the compounds studied. The docking of **III** to GluR2 and GluR5 resulted in similar conformations for the resulting complexes (the GluR5–**III** complex is shown in Fig. 7a). In this conformation, the sulfur atom accepts a hydrogen bond from the main-chain amino group of Glu705, and the N2′ of the tetrazole group interacts with the hydroxyl group of Thr655. In addition, water molecule w1 stabilizes the ligand binding conformation. The observed interaction between the sulfur atom and the amino group can be verified with ligand **VI** (Fig. 2). **VI** is otherwise similar to **III**, but instead of a $–CH_2–CH_2–S$-linker, **VI** contains a $–CH_2–CH_2–CH_2$-linker. The binding affinity of **VI** is ~7-fold lower than that of **III** (Table 1), supporting the presence of the hydrogen bond between the sulfur atom and the main-chain amino group of Glu705. Docking to both GluR2 and the model of GluR5 does not explain the GluR5-selectivity of **III**, as the ligand binding conformations and interactions with both receptors are highly similar.

During the MD simulation of GluR2–**III**, the receptor conformation does not change as much as was seen for the GluR2–**I** and GluR2–**II** complexes, only a slight rotation of S2 against S1 is seen. This rotation together with the change of the tetrazole ring orientation, due to the packing of Leu650 against planar face of tetrazole, allows the formation of one new weak electrostatic interaction (not an optimal hydrogen bond) between N3′ of the tetrazole ring and the main-chain amino group of Thr655 (Fig. 7b). At the same time, the interaction with the hydroxyl group of Thr655 weakens (Table 3). All other interactions remained the same as for the starting structure.

The MD simulation of GluR5–**III** (Fig. 7c) resulted in a conformation similar to GluR2 (Fig. 7b) except that the linker and the tetrazole ring are not as strongly bent towards helix-F as with GluR2 and the orientation of the tetrazole ring is different than with GluR2 (see Figs. 7b and 7c). This extended orientation of the linker is possible because of the smaller valine at position 650 in GluR5 instead of the bulkier leucine in GluR2. Valine in GluR5 allows the ligand to penetrate deeper into the cavity formed by helix-F and helix-H. Despite the more extended conformation of **III** in GluR5 than with GluR2 and in the starting structure, during the MD simulation the interactions remain similar as at the beginning of the simulation, but the extended conformation is energetically more favorable than that resulted from docking or MD simulation with GluR2. The calculated internal energy for ligand **III** in the conformation seen in the complex with GluR5 is 9.0 kcal mol^{-1} more favorable than the conformation seen with GluR2 (Table 2). Accordingly, it seems that the 17-fold difference in binding affinity between GluR2 and GluR5 results mainly from the internal energy of the ligand. Also the differences in other sequence positions of GluR2 and GluR5 might affect slightly into the differences in ligand binding affinities: (i) similarly as for ligand **I** the Met708 in GluR2 packs against the core of the ligand (Fig. 7b), while Ser708 in GluR5 cannot do this, (ii) similarly as in the case of GluR2–**II**, Tyr702 in GluR2 stabilizes the water w3 position and might contribute favorably to the enthropy contribution of ligand binding, while leucine in equivalent position in GluR5 cannot do this.

Ligand IV

Ligand **IV** has the highest selectivity among the studied ligands. The K_i for GluR5 is 156 nM *versus* 117 μM for GluR2, which means that **IV** binds 750 times stronger to GluR5 than to GluR2 (Table 1). In contrast to **I–III**, an imidazole group is found in **IV** instead of the tetrazole group (Fig. 2). The docking of **IV** into GluR2 resulted in a conformation where the 3′ nitrogen of the imidazole ring interacts with the main-chain amino group of Glu705, and the carboxylate substituent of the imidazole ring interacts with the hydroxyl group of Thr655 (Fig. 8a). In addition, water molecule w1 stabilizes the ligand conformation. In this conformation, however, the hydrophobic side chain of Leu650 forms unfavorable interactions with the negatively charged carboxylate group. Docking of **IV** into GluR5 resulted in a similar conformation as seen with GluR2 except that the unfavorable interaction between the hydrophobic side chain and the carboxylate group does not exist, again due to the presence of the smaller valine (650) in GluR5 as opposed to the bulkier leucine of GluR2 (Fig. 8b).

During the MD simulation of the GluR2–**IV** complex, the imidazole ring of the ligand rotates such that the hydrophobic face of the imidazole ring is positioned towards leucine, in contrast to the situation at the beginning of the simulation where the negatively charged carboxylate group pointed towards leucine (Figs. 8a and 8c). At the same time, the side chain of leucine moves away giving more space for the imidazole ring. Due to the change in the orientation of the imidazole ring, the interaction of the 3′ nitrogen atom with the main-chain amino group of Glu705 is lost and optimal interactions between carboxylate substituent and the N-terminus of helix-F cannot be formed (Table 3). Accordingly, based on the conformations obtained from docking and MD simulation, it seems that **IV** does not find a conformation which would fit into GluR2, nor can the receptor adjust its conformation to fit the ligand. This observation is consistent with experimentally observed very poor binding of **IV** to GluR2 (Table 1).

In contrast to that what is seen with GluR2 (Fig. 8c), in the MD simulation of the GluR5–**IV** complex the ligand remains in the same orientation as the starting structure (Fig. 8D). This orientation of the imidazole ring is possible because of the leucine/valine sequence difference at sequence position 650. In the GluR5–**IV**

complex, the receptor conformation changes from that of the starting structure, in which helix-F moves towards helix-H. This movement is not seen with the GluR2–**IV** complex, possibly due to the very different ligand conformation for molecule **IV**. The movement of helix-F towards helix-H allows the carboxylate group of the imidazole ring to form hydrogen bonds with the amino and hydroxyl groups of both Ser654 and Thr655 (Fig. 8d; Table 3). In addition, the 3′ nitrogen of the imidazole ring can form an ideal hydrogen bond with the main-chain amino group of Glu705 (Table 3). Thus, and in contrast to GluR2, **IV** fits very nicely into the ligand binding pocket of GluR5, forming five optimal hydrogen bonds (Table 3).

The intramolecular energies for ligand **IV** are practically same in both complexes (Table 2). Therefore the differences in the ligand binding energies (Table 1) must result from the intramolecular energy of the protein and/or from the differences in the protein–ligand interactions. As the interactions for GluR5–**IV** are better, it can be assumed that in this case the differences in the protein–ligand interactions between these two receptors are mainly responsible for the difference seen in the ligand binding affinities (Table 1). In addition to the effect of the Leu → Val (GluR2 → GluR5) difference, the differences at sequence positions 702 (GluR2: tyrosine; GluR5: leucine) and 708 (GluR2: methionine; GluR5: serine) might affect the ligand binding energies. The effect of position 708 is similar to those explained for ligands **I** and **III**: methionine in GluR2 packs against the core of the ligand (Fig. 8c), while serine in GluR5 cannot do that. Tyr702 in GluR2 has unfavorable interaction with the 2′ CH-group of imidazole-ring of **IV**, while Leu702 in GluR5 does not have this problem.

Ligand V

Ligand **V** has a 3′-carboxy-phenyl substituent directly attached to the decahydroisoquinoline ring. Ligand **V** binds very poorly to GluR2 and with moderate affinity to GluR5. The docking of **V** into GluR2 and GluR5 resulted in very similar conformations; the GluR5–**V** complex is shown in Fig. 9a. In this conformation, the carboxylate group forms a hydrogen bond with the hydroxyl group of Thr655 but the hydrophophic face of the phenyl ring is positioned towards the main-chain amino group of Glu705, forming an unfavorable interaction. In addition, in GluR2 the hydroxyl group of Thr686 points directly towards the phenyl ring, but this unfavorable interaction is not present in GluR5 where threonine is replaced by serine. However, the absence of one unfavorable interaction is not enough to explain the observed 37-fold difference in binding of **V** to GluR2 and GluR5.

During the MD simulations of the GluR2 and GluR5 complexes with **V**, helix-F moves closer to helix-H in the same way as seen with the GluR5–**IV** complex. Due to the movement of helix-F, the carboxylate group on the phenyl ring can form two hydrogen bonds and two weak interactions with receptor (Figs. 9b and 9c): with the hydroxyl group and the main-chain amino group of Thr655, and with the hydroxyl group and main-chain amino group of Ser654 (Table 3). In addition, water molecules w1 and w2 stabilize the ligand conformations. The ligand adopts a different conformation in GluR5 and GluR2. In GluR5, the plane of the phenyl ring of the ligand turns from the perpendicular orientation to the diagonal orientation relative to the plane of the decahydroisoquinoline ring (Fig. 9c). In GluR2, the plane of the phenyl ring, in turn, remains perpendicular to the plane of the bicyclical ring as in the starting structure (Fig. 9b). The different orientations of the phenyl ring can be attributed to the leucine/valine sequence difference at position 650. In GluR2, the side chain of leucine blocks the diagonal orientation of the phenyl ring, which is accessible to GluR5 with the smaller valine side chain- the side chain packs nicely against the phenyl ring. Due to the diagonal orientation of the phenyl ring in GluR5, the polar amino group of Glu705 no longer points towards the hydrophobic phenyl ring, whereas in GluR2 this unfavorable interaction remains. In addition, two other unfavorable interactions are present in GluR2, because the hydroxyl groups of Tyr702 and Thr686 point towards the phenyl ring. Furthermore, in GluR5 the space between the ligand and Glu705 is occupied by Met704, unlike for GluR2 where leucine is found (Figs. 9b and 9c). The side chain of Val650 also packs nicely against the side of phenyl ring.

Accordingly, with both receptors, the 3′ carboxylate group forms nearly the same interactions with helix-F but the ligand fits better into GluR5: Met704 fills the empty space between the phenyl ring and Glu705 and the diagonal orientation of the phenyl ring removes the unfavorable interaction with Glu705, and Val650 packs against the phenyl ring. The sequence difference at position 708 (GluR2: methionine; GluR5: serine) does not have significant role in ligand binding selectivity. The diagonal orientation of the ligand seen with GluR5 is 4.2 kcal mol^{-1} more favorable than the perpendicular conformation in GluR2 (Table 2). However, ligand **V** does not fit as nicely to GluR5 as ligand **IV** does, and **V** lacks the interaction with the main-chain amino group of Glu705. Based on this, the difference in the experimental binding affinities, 156 nM for **IV** and 1010 nM for **V**, can be understood.

Molecular dynamics simulation of ligand-free GluR2

To verify that the observed receptor movements are possible, MD-simulation for ligand-free GluR2 was done for antagonist receptor complex without an antagonist ligand (*i.e.* GluR2–ATPO crystal structure without ATPO). During the simulation, the receptor conformation varies between the starting structure, which is from the GluR2–ATPO complex (Fig. 10: orange trace) to conformation, which is highly similar to that of the crystal structure of NR1 with bound antagonist ligand DCKA (Fig. 10: blue trace). The receptor conformations seen in the simulated

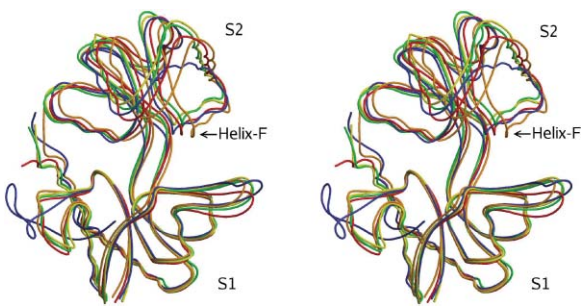

Fig. 10 During the MD simulation of ligand-free GluR2, the receptor conformation changes between the starting structure (GluR2 X-ray structure; orange trace) and conformation similar to that of X-ray structure of NR1 (blue trace), *e.g.* after 310 ps (yellow trace) receptor resembles the conformation of NR1, while after 810 ps (green trace) and 2150 ps (red trace) receptor conformation is between the starting structure and that of NR1. Figure was prepared by using coil-drawing option in Molscript.[67] This option was used for clarity.

Table 3 Polar interactions between the *R*-groups of the ligands and receptor during MD-simulation

Ligand	Thr655NH	Thr655OH	Glu705NH	Ser654NH	Ser654OH	W1	W2
GluR2							
I[a]	N4′, w/−	N3′, w/−	N1′, −/w	—	—	N3′	N2′
II	N4′	N3′	N2′, w	SO2	—	N3′	N3′
III	N3′, w	N2′, w	S	—	—	N2′	—
IV	O1, w	O1, w	—	—	—	O1	N3′
V	O1	O1, w	—	O2	O2, w	O1	O1
GluR5							
I	—	N3′	—	—	—	N3′	N2′
II	—	N3′	—	SO2	—	N3′	N3′
III	N2′, w	N1′	S	—	—	N2′, w	—
IV	O1	O1	N3′	O2	O2	—	—
V	O1	O1	—	O2	O2	O1	O1

Mean interactions of 44 structures during the last 1 ns of the whole simulation time (time intervals of 22.5 ps). The standard deviations of interaction distances and angles were 0.1–0.3 Å and 10–25°, respectively. The hydrogen bonds are considered to be strong, when the distance between heavy atoms <3.3 Å and the hydrogen bond angle (X) $-45° \leq X \leq +45°$ between D–H–A. w indicates weak polar interaction (distance between heavy atoms 3.3 Å–4.5 Å or the hydrogen bond angle does not fulfill criteria set to the strong hydrogen bond).[a] The position of the tetrazole ring easily changes due to the flexible linker effect on the interactions; *i.e.* when interactions Thr655NH–N4′ and Thr655OH–N3′ are enforced, Glu705NH–N1′ is, in turn, weakened and *vice versa.*

receptor–ligand complexes were observed in the simulation of the ligand-free GluR2 (compare Figs. 5c–d and Figure 10). Accordingly, the conformational changes observed for the receptor suggest that the "open" *i.e.* antagonist bound form of the iGluR receptors are inherently flexible.

Binding of ligands to GluR1,3,4

The binding data for **I** and **IV** are available for all AMPA receptors.[10] Both of these ligands have a slightly higher affinity for GluR1 and GluR2 than for GluR3 and GluR4.[10] This difference can be ascribed to position 702 where GluR1 and GluR2 have tyrosine and GluR3 and GluR4 have phenylalanine (Fig. 3): Tyr702 can stabilize ligand binding either *via* a direct hydrogen bond or through an intervening water molecule (data not shown).

Binding of ligands to GluR6 and GluR7

Even though GluR7 has a binding site nearly identical to that of GluR5, none of the decahydroisoquinoline derivatives binds well to GluR7 and none of the ligands binds to GluR6.[9,10,43] This binding difference can be attributed to the sequence difference at position 686. Both GluR6 and GluR7 have asparagine at 686, which blocks the binding of the decahydroisoquinoline in a similar way as we described previously for several agonist molecules.[44] In addition, GluR6 has alanine at the position 480 and since the NH_2^+ group of the decahydroisoquinolines is predicted to donate hydrogen bonds to the main-chain oxygen atom of Pro478 and the side-chain hydroxyl group of Thr480, the binding affinity for GluR6 is expected to be lower than for GluR7, which is in good agreement with the experimental binding data reported for the decahydroisoquinoline derivatives.[9,10,43]

Binding of ligands to KA2 (and KA1)

A common feature of the decahydroisoquinoline derivatives is that they do not bind to the KA2 receptor (K_i is always >100000 nM), unfortunately these data are available only for small number of molecules.[9,43,45] The sequence difference at the position 478 (Fig. 3) most likely alters the backbone conformation of the preceding Ala477, exposing an additional main-chain oxygen atom towards the ligand binding site and thus towards the hydrophobic decahydroisoquinoline. This altered backbone conformation affects the conformation of Tyr450 as well, thus affecting the packing of the decahydroisoquinoline moiety of the ligands against the S1 domain.[44] In addition, the sequence difference at position 650 can have a drastic effect on ligand binding: while AMPA receptors have leucine and GluR5–7 have valine, KA1–2 have isoleucine at this position. As already shown the leucine/valine difference at position 650 is highly important for subtype selective ligand binding and it is logical to expect that the isoleucine at that position has clear impact for binding.

Methods

Structural modeling

The three-dimensional structure of the GluR2 S1S2 construct in complex with ATPO (PDB access code: 1n0t[12]), was obtained from the Protein Data Bank.[46] The sequence alignment of human GluR1–4 (AMPA-receptors), GluR5–7 and KA1–2 (KA-receptors) was made using Malign[47] in the Bodil Modeling Environment[33] using a structure-based sequence comparison matrix[48] with a gap formation penalty of 40. Malign constructs a multiple-sequence alignment from pairwise alignments according to a tree relating the sequences being matched.

The program Homodge in Bodil was used to construct 3D model structures for each receptor LBD (except GluR2 where the X-ray structure was used) by keeping the side-chain conformations of all identical residues fixed and by maintaining the corresponding torsion angles of similar residues in the alignment. Here, the sequence identity varies from approximately 90% (among the AMPA receptors) to about 50% (between GluR2 and the KA receptors). The intramolecular interactions of the amino acids in the vicinity of the ligand binding site that are different from those in the template structure were optimized by using the amino acid side-chain rotamer library[49] incorporated within BODIL. Hydrogen atoms for all protein structures and models were added using the program Reduce.[50]

Ligand structures

Ligand structures were optimized quantum mechanically with Gaussian03[51] at the HF/6-31 + G** level, first *in vacuo* and then using a continuum solvent model (water, using the PCM model of Gaussian03).

Possible low-energy conformations for the ring-system of the decahydroisoquinolines were produced with the 2D–3D conversion program Corina,[38,39] using an energy window of 60 kcal mol^{-1}.

Hybridization and protonization of the ligands were confirmed by examining the available pK_a values and similar (sub)structures using Beilstein (MDL Information. Systems, Inc).

Ligand docking

Ligands were docked flexibly into the AMPA/KA receptors with Gold 2.1.[52,53] The search area was limited to a 15 Å radius sphere centered at the binding site.

Molecular dynamics

The ligand–receptor complex structures obtained from the docking studies were used as starting structures for the ligand–receptor MD simulations. For ligand-free simulation, the receptor structure of GluR2–ATPO complex, without bound ATPO, was used as a starting structure.[12] Water molecules within a 4.0 Å distance of the ligand in the X-ray structure of GluR2 with bound ATPO were included in starting structures (water molecules with similar positions were also included in the GluR5–ligand complexes). The force field parameters for the protein were taken from the parm99 parameter set[54] of Amber 8[55] and for the ligands from the gaff parameter set.[56] Missing parameters and atom types of the ligands were generated using the Antechamber module of Amber 8. The quantum mechanically optimized structures of the ligands were used. The electrostatic potentials of the ligands were obtained from *ab initio* quantum mechanical single point energy calculations (HF/6-31 + G* with Gaussian03[51]) performed for the structure obtained from the solution optimization. Atom-centered point charges for corresponding atoms were generated from the electrostatic potential using the RESP methodology.[57–59] The charges of chemically equivalent atoms were set to equal values.

The ligand–receptor complexes were solvated with a rectangular box of TIP3P waters extending 13 Å in all dimensions around the solute using the Leap[60] module of Amber 8. The number of water molecules in simulations were GluR2: 14387; GluR2–**I**: 14383; GluR2–**II**: 14385; GluR2–**III**: 14383; GluR2–**IV**: 14387; GluR2–**V**: 14386; GluR5–**I**: 13500; GluR5–**II**: 13522; GluR5–**III**: 13500; GluR5–**IV**: 13512; GluR5–**V**: 13556. The system was then neutralized by adding the appropriate number of counter ions (GluR2 *apo*: four chlorides; GluR2–**I** ligand complexes: three chlorides; GluR5–ligand complexes: one sodium).

Energy minimizations and molecular dynamics simulations were performed using the PMEMD module of Amber 8. Equilibration was performed using the following procedure. In the first step, the hydrogen atoms in the system were minimized using the steepest decent algorithm (1000 steps) keeping the rest of the system fixed, followed by a similar relaxation of the water molecules. In the MD run, the system was heated from an initial temperature of 100 K to 300 K in 30 ps, and thereafter the temperature was maintained at 300 K. After relaxation, the system was energy minimized for 1000 steps. Finally, unrestrained molecular dynamics simulation of the whole system was started by heating up the whole system as done in the equilibration MD simulation of the water molecules. After that, the production simulations of 2.1–3.5 ns at constant temperature (300 K) and pressure (1 atm) were started. For GluR2–**I** complex a longer simulation (3.5 ns) was performed in order to see if longer simulations would be required. Since the trajectories were stable and no significant conformational changes were not seen during the extension of the simulation, 2.1 ns simulation time were considered to be long enough. All simulations were run using a 1.5 fs step time. A cutoff of 8.0 Å was used for van der Waals interactions and the long-range electrostatic interactions were treated using the particle mesh Ewald summation method[61–64] with a charge grid spacing of ~1.0 Å. Bonds containing hydrogen atoms were constrained using the SHAKE algorithm.[65]

Trajectory analyses

Trajectories obtained from the MD simulations were analyzed with the ptraj module of Amber 8.

Internal energies of ligands

For each compound, 27 snapshot structures, containing only ligand coordinates, were collected at 15 ps intervals over the final 400 ps of the simulation. Single-point energies for these ligand conformations were calculated quantum mechanically at the B3LYP/6-31 + G* level with Gaussian03.[51]

Ligand binding data

The ligand binding data for enantiomerically pure decahydroisoquinolines, measured on *homomeric* iGluRs, were taken from the literature.[7,10]

Figures

Fig. 3 was prepared by using Alscript[66] and figures 1, 4–10 by using Bodil,[33] Molscript[67] and Raster3D.[68]

Conclusions

With regard to receptor binding, the studied ligands have several features in common. The decahydroisoquinoline moiety forms similar interactions in all cases. In addition, all negatively charged R-groups: tetrazole (**I–III**), carboxylate groups (**IV–V**) and the oxygen atoms of the sulfonyl group (**II**) interact with the positively charged N-terminus of helix-F. These results are consistent with the crystal structures of GluR2 with other types of bound ligands (with the exception of DNQX), where negatively charged groups are observed to interact with the helix-F.[11] Another important interaction that is observed is with the main-chain amino group of Glu705. This interaction is seen in the GluR2–**III**, GluR5–**III** and GluR5–**IV** complexes and is quite often seen in the crystal structures too (*e.g.* GluR2–AMPA[11]). However, in the complexes with **I**, **II** and **V** water molecules occupy this interaction site in a similar way as w4 in the crystal structure of GluR2 with bound ATPO (see Fig. 1). Water molecules w1 and w2 seen in the crystal structures (*e.g.* GluR2–ATPO; Fig. 1) are observed in all of the ligand–receptor complex structures obtained from MD simulations (Figs. 5–9). The other water molecules seen in crystal structures, w3 and w5 (Fig. 1), are, in turn, replaced by some of the ligands.

The ligand conformations are strongly dependent on the sequence differences between GluR2 and GluR5. Especially, the leucine (in GluR2)-valine (in GluR5) difference at position 650 has a strong influence on the ligand conformation and in this way also on selective ligand binding to the receptors, depending on the length of the linker. The ligand with the longest linker (**III**) has the highest sensitivity to the size of the side chain at this position. The smaller valine in GluR5 allows the linker to adopt a more extended conformation than the bulkier leucine in GluR2, contributing 9.0 kcal mol^{-1} to the stability of the complex in GluR5 (Table 2). In contrast, with linkers of two connecting atoms (**I–II**), the influence of valine is the opposite: the tetrazole ring can penetrate deeper into the cavity formed by helices F and H in GluR5 because of smaller valine, and these results in a loss of interactions. In addition, the larger side chain of leucine (GluR2) packs better on the top of the tetrazole ring than the smaller side chain of valine (GluR5); in the case of **II**, having accordingly a positive impact on the total ligand binding energy. With the smaller ligands, **IV** and **V**, leucine prevents the imidazole (**IV**) or phenyl (**V**) ring adopting orientations that would allow the best possible interactions with the receptor, whereas valine allows favorable conformations. With **IV**, the observed binding conformation from the MD simulations have similar internal energies, but with **V** the conformation in GluR5 is 4.2 kcal mol^{-1} more favorable than that in GluR2 (Table 2). The observation of the importance of the leucine/valine difference on the ligand binding conformation is not new. For example, this sequence position has been shown to be responsible for the pharmacological differences of the ligand kainate towards the AMPA and KA receptors[69] and also for agonist ligand binding selectivity.[70–72]

During the MD simulations, the receptor structures alter their conformations, however, the magnitude and manner of the conformational change depends on the bound ligand and the receptor type (GluR2 or GluR5). During the simulation of GluR2 with bound molecules **I** and **II**, the receptor changes its conformation to resemble that of the NR1 receptor (Figs. 5c and 5d), while GluR5 alters its conformation to a much lesser extent. The greater degree of conformational change in GluR2 allows **I** and **II** to adopt a more favorable conformation in contrast to GluR5. With the largest ligand, **III**, neither of receptors changes conformation. Ligands **IV** and **V** are much smaller than **I–III**. With these ligands, the movement of the receptors differs from that of the larger ligands. In comparison to the X-ray structure of GluR2–ATPO complex, helix-F moves towards helix-H in the GluR5–**IV**, GluR2–**V** and GluR5–**V** complexes. With GluR2–**IV**, this kind of movement is not seen due to the different ligand conformation. The changes in the receptor conformation that are dependent on bound ligand, which are seen in this study, are not seen in the currently available X-ray structures of AMPA/KA receptors.

Although, the results described here are based on single trajectories for each protein–ligand complexes, the results obtained can be assumed to be reliable because of the following reasons. (1) The ligands **I** and **II** have the same core structure and the length of R-groups are similar (Fig. 2). When these ligands are bound to GluR2 and GluR5, similar changes in the receptor conformations are seen during the MD simulations. Accordingly, similar results were obtained from four independent trajectories. (2) For ligand **II**, two distinct starting conformations were used with GluR2 and GluR5 (Fig. 6a and 6c). However, during the MD simulation both starting conformations ended up to highly similar conformation (Fig. 6b and 6d). (3) The simulation of ligand-free antagonist form of GluR2 varies between conformations seen for the crystal structures of GluR2 with bound ATPO and NR1 with bound DCKA (Fig. 10). In addition, those receptor conformations, which were seen in the receptor–ligand simulations, were also observed in the ligand-free simulation. Accordingly, the observed dynamics of the ligand-free antagonist form of the receptor suggests that the receptor is inherently flexible. In order to investigate if the receptor starting conformations effect on the behaviour of the receptor during MD simulations, several starting conformations for the receptor should have been used. However, in the case of GluR-antagonist complexes, it is very difficult to use any other sensible starting conformation for the receptor beside those used, since the only available crystal structures for GluR2 and GluR5 with bound antagonist ligands are the complexes of GluR2 with bound ATPO and DNQX that are highly similar to each others. The usage of agonist ligand complexes that are numerous and available for both GluR2 and GluR5 cannot be used as the receptor structures are more "closed", which reflects the size of the binding cavity, and thus, the positioning of studied antagonist ligands into the binding cavity is impossible. Accordingly, since several independent trajectories gave consistent results in the respect of the receptor movement and similar conformations are also seen in the X-ray structures of iGluRs, our hypothesis that the "open" (*i.e.* antagonist) forms of iGluR receptors are flexible and the receptor conformation may change upon the shape and size the ligand bound can be assumed to be reasonable.

In summary, the binding mode of decahydroisoquinoline derivatives is a complex problem, affected by many different factors. The results obtained here show reasonable binding modes for these ligands, which are consistent with the experimentally observed binding affinities. In addition, the changes in the receptor conformation depending on the bound ligand give new information about receptor flexibility upon antagonist ligand binding. Thus, this study provides a basis for understanding receptor–ligand selectivity and yields insight applicable to the design of novel selective ligands.

Acknowledgements

This study was supported by grants from the Åbo Akademi University (to L.S.) and the Sigrid Jusélius Foundation (to M.S.J.). Access to Gold and Gaussian03 was provided by the Centre for Scientific Computing (CSC, Espoo, Finland).

References

1 P. Conti, M. De Amici and C. De Micheli, *Mini-Rev. Med. Chem.*, 2002, **2**, 177–184.
2 T. B. Stensbol, U. Madsen and P. Krogsgaard-Larsen, *Curr. Pharm. Des.*, 2002, **8**, 857–872.
3 W. Danysz and A. C. Parsons, *Pharmacol. Rev.*, 1998, **50**, 597–664.
4 R. Dingledine, K. Borges, D. Bowie and S. F. Traynelis, *Pharmacol. Rev.*, 1999, **51**, 7–61.
5 H. Brauner-Osborne, J. Egebjerg, E. O. Nielsen, U. Madsen and P. Krogsgaard-Larsen, *J. Med. Chem.*, 2000, **43**, 2609–2645.
6 G. J. Lees, *Drugs*, 2000, **59**, 33–78.
7 M. J. O'Neill, A. Bond, P. L. Ornstein, M. A. Ward, C. A. Hicks, K. Hoo, D. Bleakman and D. Lodge, *Neuropharmacology*, 1998, **37**, 1211–1222.
8 M. J. O'Neill, L. Bogaert, C. A. Hicks, A. Bond, M. A. Ward, G. Ebinger, P. L. Ornstein, Y. Michotte and D. Lodge, *Neuropharmacology*, 2000, **39**, 1575–1588.

9 I. Smolders, Z. A. Bortolotto, V. R. Clarke, R. Warre, G. M. Khan, M. J. O'Neill, P. L. Ornstein, D. Bleakman, A. Ogden, B. Weiss, J. P. Stables, K. H. Ho, G. Ebinger, G. L. Collingridge, D. Lodge and Y. Michotte, *Nat. Neurosci.*, 2002, **5**, 796–804.
10 S. A. Filla, M. A. Winter, K. W. Johnson, D. Bleakman, M. G. Bell, T. J. Bleisch, A. M. Castano, A. Clemens-Smith, M. del Prado, D. K. Dieckman, E. Dominguez, A. Escribano, K. H. Ho, K. J. Hudziak, M. A. Katofiasc, J. A. Martinez-Perez, A. Mateo, B. M. Mathes, E. L. Mattiuz, A. M. Ogden, L. A. Phebus, D. R. Stack, R. E. Stratford and P. L. Ornstein, *J. Med. Chem.*, 2002, **45**, 4383–4386.
11 N. Armstrong and E. Gouaux, *Neuron*, 2000, **28**, 165–181.
12 A. Hogner, J. R. Greenwood, T. Liljefors, M. L. Lunn, J. Egebjerg, I. K. Larsen, E. Gouaux and J. S. Kastrup, *J. Med. Chem.*, 2003, **46**, 214–221.
13 H. Furukawa and E. Gouaux, *EMBO J.*, 2003, **22**, 2873–2885.
14 R. L. McFeeters and R. E. Oswald, *Biochemistry*, 2002, **41**, 10472–10481.
15 E. Gouaux, *J. Physiol.*, 2004, **554**, 249–253.
16 R. Abele, D. Svergun, K. Keinänen, M. H. Koch and D. R. Madden, *Biochemistry*, 1999, **38**, 10949–10957.
17 R. Abele, K. Keinänen and D. R. Madden, *J. Biol. Chem.*, 2000, **275**, 21355–21363.
18 R. L. McFeeters, G. V. Swapna, G. T. Montelione and R. E. Oswald, *J. Biomol. NMR*, 2002, **22**, 297–298.
19 L. Zeng, L. Lu, M. Muller, E. Gouaux and M. M. Zhou, *J. Mol. Neurosci.*, 2002, **19**, 113–116.
20 L. Zeng, C. H. Chen, M. Muller and M. M. Zhou, *J. Mol. Neurosci.*, 2003, **20**, 345–348.
21 L. Zeng, K. Chen, M. Muller and M. M. Zhou, *J. Mol. Neurosci.*, 2004, **24**, 81–84.
22 E. R. Valentine and A. G. Palmer, 3rd, *Biochemistry*, 2005, **44**, 3410–3417.
23 Q. Cheng, S. Thiran, D. Yernool, E. Gouaux and V. Jayaraman, *Biochemistry*, 2002, **41**, 1602–1608.
24 Q. Cheng and V. Jayaraman, *J. Biol. Chem.*, 2004, **279**, 26346–26350.
25 M. Du, S. A. Reid and V. Jayaraman, *J. Biol. Chem.*, 2005, **280**, 8633–8636.
26 J. Mendieta, G. Ramirez and F. Gago, *Proteins: Struct., Funct., Genet.*, 2001, **44**, 460–469.
27 Y. Arinaminpathy, M. S. Sansom and P. C. Biggin, *Biophys. J.*, 2002, **82**, 676–683.
28 M. Kubo and E. Ito, *Proteins*, 2004, **56**, 411–419.
29 M. Kubo, E. Shiomitsu, K. Odai, T. Sugimoto, H. Suzuki and E. Ito, *Proteins*, 2004, **54**, 231–236.
30 O. T. Pentikäinen, U. Pentikäinen, L. Settimo and M. S. Johnson, *unpublished work*.
31 V. A. Ostrovskii, G. I. Koldobskii, N. P. Shirokova and V. S. Poplavskii, *Chem. Heterocycl. Compd. (Engl. Transl.)*, 1981, **4**, 559–562.
32 K. Takahashi, I. Kimura, Y. Takei, T. Zaima and K. Mitsuhashi, *Nippon Kagaku Kaishi*, 1975, **9**, 1530–1531.
33 J. V. Lehtonen, D.-J. Still, V.-V. Rantanen, J. Ekholm, D. Björklund, Z. Iftikhar, M. Huhtala, S. Repo, A. Jussila, J. Jaakkola, O. T. Pentikäinen, T. Nyrönen, T. Salminen, M. Gyllenberg and M. S. Johnson, *J. Comput. Aided Mol. Des.*, 2004, **18**, 401–419.
34 P. Naur, B. Vestergaard, L. K. Skov, J. Egebjerg, M. Gajhede and J. S. Kastrup, *FEBS Lett.*, 2005, **579**, 1154–1160.
35 M. L. Mayer, *Neuron*, 2005, **45**, 539–552.
36 F. H. Allen, *Acta Crystallogr., Sect. B: Struct. Sci.*, 2002, **58**, 380–388.
37 J. C. Gilbert, S. Redshaw, H. S. Simmonite, W. A. Thomas and I. W. A. Whitcombe, *J. Chem. Soc., Perkin Trans. 2*, 1993, **3**, 475–479.
38 J. Sadowski and J. Gasteiger, *Chem. Rev.*, 1993, **93**, 2567–2581.
39 J. Sadowski, J. Gasteiger and G. Klebe, *J. Chem. Inf. Comput. Sci.*, 1994, **34**, 1000–1008.
40 N. Armstrong, Y. Sun, G. Q. Chen and E. Gouaux, *Nature*, 1998, **395**, 913–917.
41 M. H. Nanao, T. Green, Y. Stern-Bach, S. F. Heinemann and S. Choe, *Proc. Natl. Acad. Sci. U. S. A.*, 2005, **102**, 1708–1713.
42 P. Kollman, I. Massova, C. Reyes, B. Kuhn, S. Huo, L. Chong, M. Lee, T. Lee, Y. Duan, W. Wang, O. Donini, P. Cieplak, J. Srinivasan, D. Case and T. Cheatham, III, *Acc. Chem. Res.*, 2000, **33**, 889–897.
43 Z. A. Bortolotto, V. R. Clarke, C. M. Delany, M. C. Parry, I. Smolders, M. Vignes, K. H. Ho, P. Miu, B. T. Brinton, R. Fantaske, A. Ogden, M. Gates, P. L. Ornstein, D. Lodge, D. Bleakman and G. L. Collingridge, *Nature*, 1999, **402**, 297–301.
44 O. T. Pentikäinen, L. Settimo, K. Keinänen and M. S. Johnson, *Biochem. Pharmacol.*, 2003, **66**, 2413–2425.
45 D. Bleakman, M. R. Gates, A. M. Ogden and M. Mackowiak, *Curr. Pharm. Des.*, 2002, **8**, 873–885.
46 H. M. Berman, J. Westbrook, Z. Feng, G. Gilliland, T. N. Bhat, H. Weissig, I. N. Shindyalov and P. E. Bourne, *Nucleic Acids Res.*, 2000, **28**, 235–242.
47 M. S. Johnson and J. P. Overington, *J. Mol. Biol.*, 1993, **233**, 716–738.
48 M. S. Johnson, A. C. W. May, M. A. Rodionov and J. P. Overington, *Methods Enzymol.*, 1996, **266**, 575–598.
49 S. C. Lovell, J. M. Word, J. S. Richardson and D. C. Richardson, *Proteins: Struct., Funct., Genet.*, 2000, **40**, 389–408.
50 J. M. Word, S. C. Lovell, J. S. Richardson and D. C. Richardson, *J. Mol. Biol.*, 1999, **285**, 1735–1747.
51 M. J. Frisch, G. W. Trucks, H. B. Schlegel, G. E. Scuseria, M. A. Robb, J. R. Cheeseman, J. A. Montgomery, Jr., T. Vreven, K. N. Kudin, J. C. Burant, J. M. Millam, S. S. Iyengar, J. Tomasi, V. Barone, B. Mennucci, M. Cossi, G. Scalmani, N. Rega, G. A. Petersson, H. Nakatsuji, M. Hada, M. Ehara, K. Toyota, R. Fukuda, J. Hasegawa, M. Ishida, T. Nakajima, Y. Honda, O. Kitao, H. Nakai, M. Klene, X. Li, J. E. Knox, H. P. Hratchian, J. B. Cross, V. Bakken, C. Adamo, J. Jaramillo, R. Gomperts, R. E. Stratmann, O. Yazyev, A. J. Austin, R. Cammi, C. Pomelli, J. Ochterski, P. Y. Ayala, K. Morokuma, G. A. Voth, P. Salvador, J. J. Dannenberg, V. G. Zakrzewski, S. Dapprich, A. D. Daniels, M. C. Strain, O. Farkas, D. K. Malick, A. D. Rabuck, K. Raghavachari, J. B. Foresman, J. V. Ortiz, Q. Cui, A. G. Baboul, S. Clifford, J. Cioslowski, B. B. Stefanov, G. Liu, A. Liashenko, P. Piskorz, I. Komaromi, R. L. Martin, D. J. Fox, T. Keith, M. A. Al-Laham, C. Y. Peng, A. Nanayakkara, M. Challacombe, P. M. W. Gill, B. G. Johnson, W. Chen, M. W. Wong, C. Gonzalez and J. A. Pople, *GAUSSIAN 03 (Revision C.02)*, Gaussian, Inc., Wallingford, CT, 2004.
52 G. Jones, P. Willett and R. C. Glen, *J. Mol. Biol.*, 1995, **245**, 43–53.
53 G. Jones, P. Willett, R. C. Glen, A. R. Leach and R. Taylor, *J. Mol. Biol.*, 1997, **267**, 727–748.
54 J. Wang, P. Cieplak and P. A. Kollman, *J. Comput. Chem.*, 2000, **21**, 1049–1074.
55 D. A. Case, T. A. Darden, T. E. Cheatham, III, C. L. Simmerling, J. Wang, R. E. Duke, R. Luo, K. M. Merz, B. Wang, D. A. Pearlman, M. Crowley, S. Brozell, V. Tsui, H. Gohlke, J. Mongan, V. Hornak, G. Cui, P. Beroza, C. Schafmeister, J. W. Caldwell, W. S. Ross and P. A. Kollman, *Amber 8*, University of California, San Francisco, 2004.
56 J. Wang, R. M. Wolf, J. W. Caldwell, P. A. Kollman and D. A. Case, *J. Comput. Chem.*, 2004, **25**, 1157–1173.
57 C. I. Bayly, P. Cieplak, W. D. Cornell and P. A. Kollman, *J. Phys. Chem.*, 1993, **97**, 10269–10280.
58 W. D. Cornell, P. Cieplak, C. I. Bayly and P. A. Kollman, *J. Am. Chem. Soc.*, 1993, **115**, 9620–9631.
59 P. Cieplak, W. D. Cornell, C. Bayly and P. A. Kollman, *J. Comput. Chem.*, 1995, **16**, 1357–1377.
60 C. E. A. F. Schafmeister, W. S. Ross and V. Romanovski, *The LEaP module of Amber,*University of California, San Francisco, 1995.
61 T. Darden, D. York and L. Pedersen, *J. Chem. Phys.*, 1993, **98**, 10089–10092.
62 U. Essmann, L. Perera, M. L. Berkowitz, T. Darden, H. Lee and L. G. Pedersen, *J. Chem. Phys.*, 1995, **103**, 8577–8593.
63 C. Sagui and T. A. Darden, in *Simulation and Theory of Electrostatic Interactions in Solution*, ed. L. R. P. A. G. Hummer, Melville, New York, 1999.
64 A. Toukmaji, C. Sagui, J. Board and T. Darden, *J. Chem. Phys.*, 2000, **113**, 10913–10927.
65 J.-P. Ryckaert, G. Ciccotti and H. J. C. Berendsen, *J. Comput. Phys.*, 1977, **23**, 327–341.
66 G. J. Barton, *Protein Eng.*, 1993, **6**, 37–40.
67 J. Kraulis, *J. Appl. Crystallogr.*, 1991, **24**, 946–950.
68 E. Merritt and D. Bacon, *Methods Enzymol.*, 1997, **277**, 505–524.
69 D. R. Madden, Q. Cheng, S. Thiran, S. Rajan, F. Rigo, K. Keinänen, S. Reinelt, H. Zimmermann and V. Jayaraman, *Biochemistry*, 2004, **43**, 15838–15844.
70 I. Mano, Y. Lamed and V. I. Teichberg, *J. Biol. Chem.*, 1996, **271**, 15299–15302.
71 M. Lampinen, L. Settimo, O. T. Pentikäinen, A. Jouppila, D. G. Mottershead, M. S. Johnson and K. Keinänen, *J. Biol. Chem.*, 2002, **277**, 41940–41947.
72 N. Armstrong, M. Mayer and E. Gouaux, *Proc. Natl. Acad. Sci. U. S. A.*, 2003, **100**, 5736–5741.

